A Compressive Sensing-Based Near-Field Antenna Characterization - The Bayesian Approach

M. Salucci, N. Anselmi, and A. Massa

2019/12/22

Contents

1 Near-Field Antenna Characterization Through the Bayesian Compressive Sensing (*BCS*) Approach

1.1 Parameters

Gold Antenna (Without Defects)

- Geometry : Planar array of microstrip patches on the (x, y) plane;
- Working Frequency : $f = 3.6\,[GHz]$ ($\lambda = 83.27 \times 10^{-3}\,[m]$ in free space);
- Substrate (PEC-backed) :
  - Dimensions : infinite;
  - Relative Permittivity : $\varepsilon_{r,sub} = 4.7$;
  - Loss Tangent : $tan\,\delta_{sub} = 0.014$;
  - Thickness : $h_{sub} = 0.019\,[\lambda]\ (1.6\,[mm])$;
- Microstrip patches :
  - Dimensions : $l_x \approx 0.22\,[\lambda]\ (18.16\ [mm]),\ l_y \approx 0.33\,[\lambda]\ (27.25\ [mm])$;
  - Feeding : pin-fed;
- Spacing between elements : $d_x = d_y = \frac{\lambda}{2}$;
- Number of elements in each row : $N_x = 6$;
- Number of elements in each column : $N_y = 10$;
- Total number of elements : $N = (N_x \times N_y) = 60$;
- Total size of the antenna : $L_x = 5\,[\lambda],\ L_y = 9\,[\lambda]$;
- Element excitations : $w_n^{(s)} = 1.0 + j0.0,\ n = 1, ..., N^{(s)},\ s = 1, ..., S$;

Antenna Under Test (AUT - With Defects)

1. Failures of the excitation magnitude of the 3^{rd} row;
   - Failure factor of the elements in the 3^{rd} row $(s = 3)$: $\nu^{(3)} = 0.45$;
2. Failures of the excitation phase of the 3^{rd} row;
   - Phase shift of the elements in the 3^{rd} row $(s = 3)$: $\gamma^{(3)} = \frac{\pi}{3}\,[rad]$;

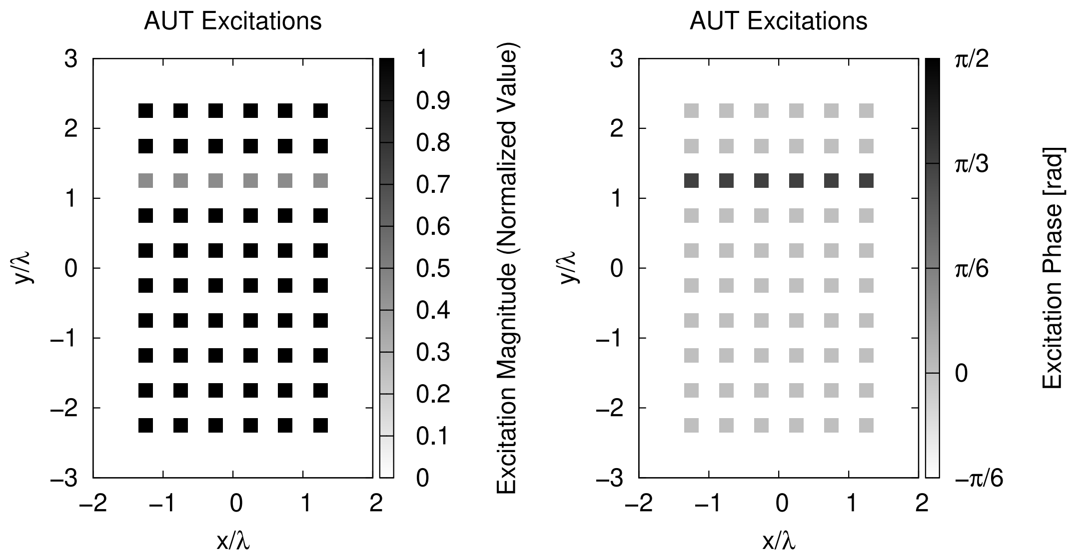

(*a*) (*b*)

Figure 1: (*a*) Magnitude of the element excitations in the *AUT* ($\nu^{(3)} = 0.45$), (*b*) phase of the element excitations in the *AUT* ($\gamma^{(3)} = \frac{\pi}{3}\,[rad]$).

Measurement Set-Up

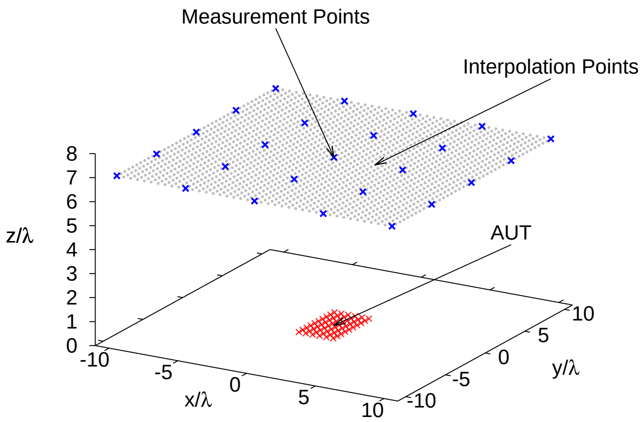

Figure 2: Disposition of the interpolation points ($T = 1681$) and of the measurement points ($M = 25$) in the near-field region of the *AUT*

- Type of measurements : near-field;
- Height of the measurement region : $H = 7\,[\lambda]$;
- Interpolation points :
  - Number of points : $T = 41 \times 41 = 1681$;
  - Coordinates : $x_t \in [-10,\, 10]\,[\lambda],\ y_t \in [-10,\, 10]\,[\lambda],\ z_t = H\,[\lambda],\ t = 1, ..., T$;
  - Interpolation step : $\Delta_{x/y}^{int} = 0.5\,[\lambda]$;
- Measurement points :
  - Coordinates : $x_m^{meas} \in [-10,\, 10]\,[\lambda],\ y_m^{meas} \in [-10,\, 10]\,[\lambda],\ z_m^{meas} = H\,[\lambda],\ m = 1, ..., M$;

- Number of points : $M_{x/y} = 5 \rightarrow M = 25$;
- Measurement step : $\Delta_{x/y}^{meas} = 5\,[\lambda]$
- Ratio between number of measurements and total number of elements : $(M/N) = 0.42$;

Measurement-by-Design Technique

- Number of generated bases : $B = 20$;
- Bases $b = 1, ..., 10$: magnitude failures in each row $(s = 1, ..., 10)$
  - Failure factor of the elements : $\nu^{(s)} \in [0.0,\, 0.5],\;\; s = 1, ..., 10$;
  - Number of simulated failure factors : $F^{(s)} = 7,\; s = 1, ..., 10$;
- Bases $b = 11, ..., 20$: phase failures in each row $(s = 1, ..., 10)$
  - Phase shift of the elements : $\gamma^{(s)} \in [0,\, \frac{\pi}{4}]\,[rad],\;\; s = 1, ..., 10$;
  - Number of simulated phase shifts: $P^{(s)} = 5,\;\; s = 1, .., 10$;
- Threshold on the singular values magnitude (normalized) : $\eta = -40\,[dB]$;
- Total number of simulated AUT configurations : $K = S \times (F^{(s)} + P^{(s)}) = 10 \times (7 + 5) = 120$;

Noise

- SNR on the measured data : $SNR = \{50;\, 40;\, 30;\, 20; 10\}\,[dB]$;
- Noise seed : $Noise\_Seed = 11$.

1.2 *BCS* Algorithm

Parameters

- Toleration factor for *BCS* solver: $Tolerance = 1 \times 10^{-8}$;
- Initial noise variance for *BCS* solver: $\eta_0^{opt_1} = 10^{-2}$, $\eta_0^{opt_2} = 5 \times 10^{-4}$. These values have been obtained as a result of a calibration procedure (see following Sec. 1.2).

Calibration of the initial noise variance (η_0)

In order to find the best value for the initial noise variance value (η_0^{opt}), the *BCS* version of the *MbD* has been run considering the following ranges of values for η_0 and SNR :

- $\eta_0 = [10^{-9}, 5{\times}10^{-9}, 10^{-8}, 5{\times}10^{-8}, 10^{-7}, 5{\times}10^{-7}, 10^{-6}, 5{\times}10^{-6}, 10^{-5}, 5{\times}10^{-5}, 10^{-4}, 5{\times}10^{-4}, 10^{-3}, 5\times 10^{-3}, 10^{-2}, 5 \times 10^{-2}, 10^{-1}, 5 \times 10^{-1}, 1, 5, 10]$;
- $SNR = [60, 50, 40, 30, 20]$.

The best value has been computed as the minimum mean near field error over the considered *SNR* values for each η_0; in formula:

$$\eta_0^{opt} = min_{\eta_0^{(i)}} \left\{ \frac{\sum_{j=1}^{N_{SNR}} \Xi_{AUT,\eta_0^{(i)}}^{(j)}}{N_{SNR}} \right\} \tag{1}$$

where

- η_0^i is the $i-th$ considered η_0 value;
- $\Xi_{AUT,\eta_0^{(i)}}^{(j)}$ is the near field error obtained considering the $i-th$ value of η_0 and the $j-th$ value of SNR;
- N_{SNR} is the total number of considered SNR values.

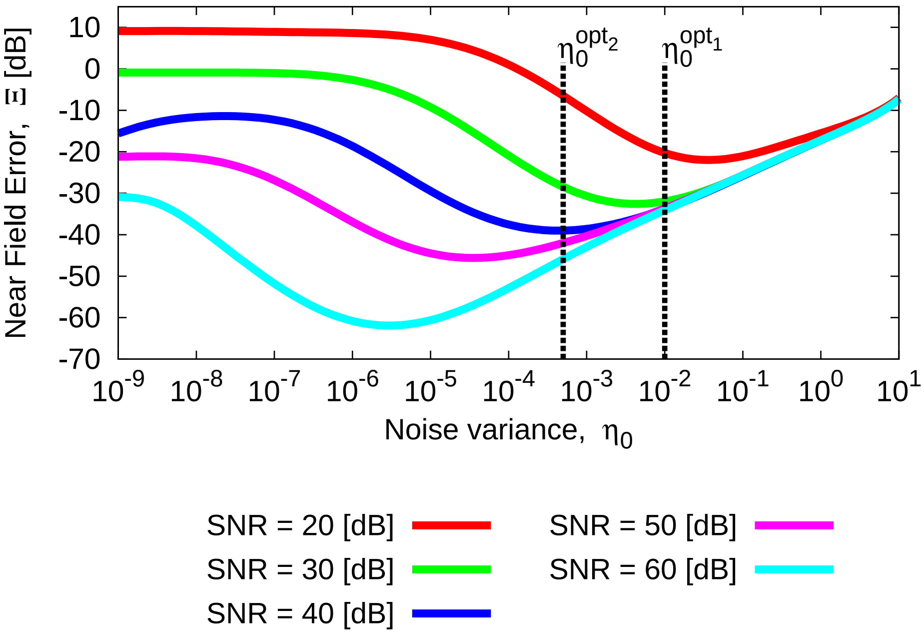

Figure 3: Initial noise variance η_0 calibration

As shown in Fig. 3 two different values of η_0 have been computed:

1. $\eta_0^{opt_1} = 10^{-2}$: this is the optimum value for the initial noise variance when all the SNR range has been considered, $SNR = [60,\ 50,\ 40,\ 30,\ 20]$;
2. $\eta_0^{opt_2} = 5 \times 10^{-4}$: this is the optimum value for the initial noise variance when SNR ranges in a restricted interval, $SNR = [60,\ 50,\ 40,\ 30]$.

1.3 Results

Behaviour of the Near-Field Error

The following Fig. 4 shows the near field error (Ξ) that the considered algorithm makes in estimating the near field of the *AUT* for different SNR values.

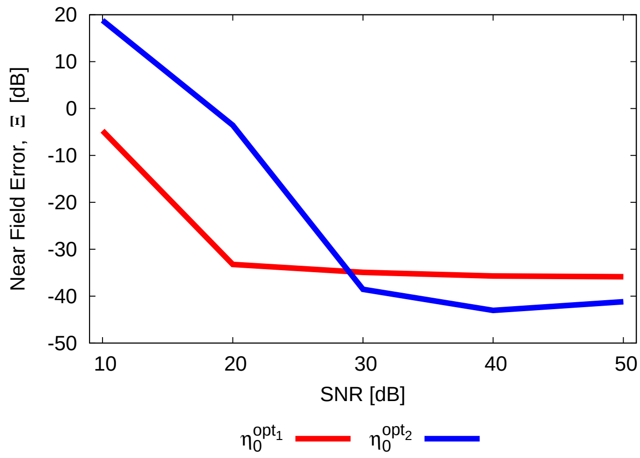

Figure 4: Near-Field Error behaviour versus *SNR* values

SNR $[dB]$	*Near Field Error,* Ξ $[dB]$	
	$\eta_0^{opt_1}$	$\eta_0^{opt_2}$
50	-35.86	-41.19
40	-35.71	-43.04
30	-34.93	-38.56
20	-33.24	-3.56
10	-4.73	18.80

Table I: Near-field error obtained at different SNR values

Observations

The results of Tab. I point out that:

- using $\eta_0^{opt_1} = 1E-2$, the *BCS* algorithm performs very good starting from $SNR = 20\,[dB]$; instead, the performance degrades when $SNR < 20\,[dB]$;
- using $\eta_0^{opt_2} = 5E-4$, the *BCS* algorithm achieves the best results when $SNR \geq 30\,[dB]$; instead, the results make worse for $SNR < 30\,[dB]$.

Which vectors in the over-complete basis have been selected?

The following Fig. 5 shows which vectors of the over-complete basis (consisting of a total of $Q = 40$ vectors) have been selected by the *BCS* solver.

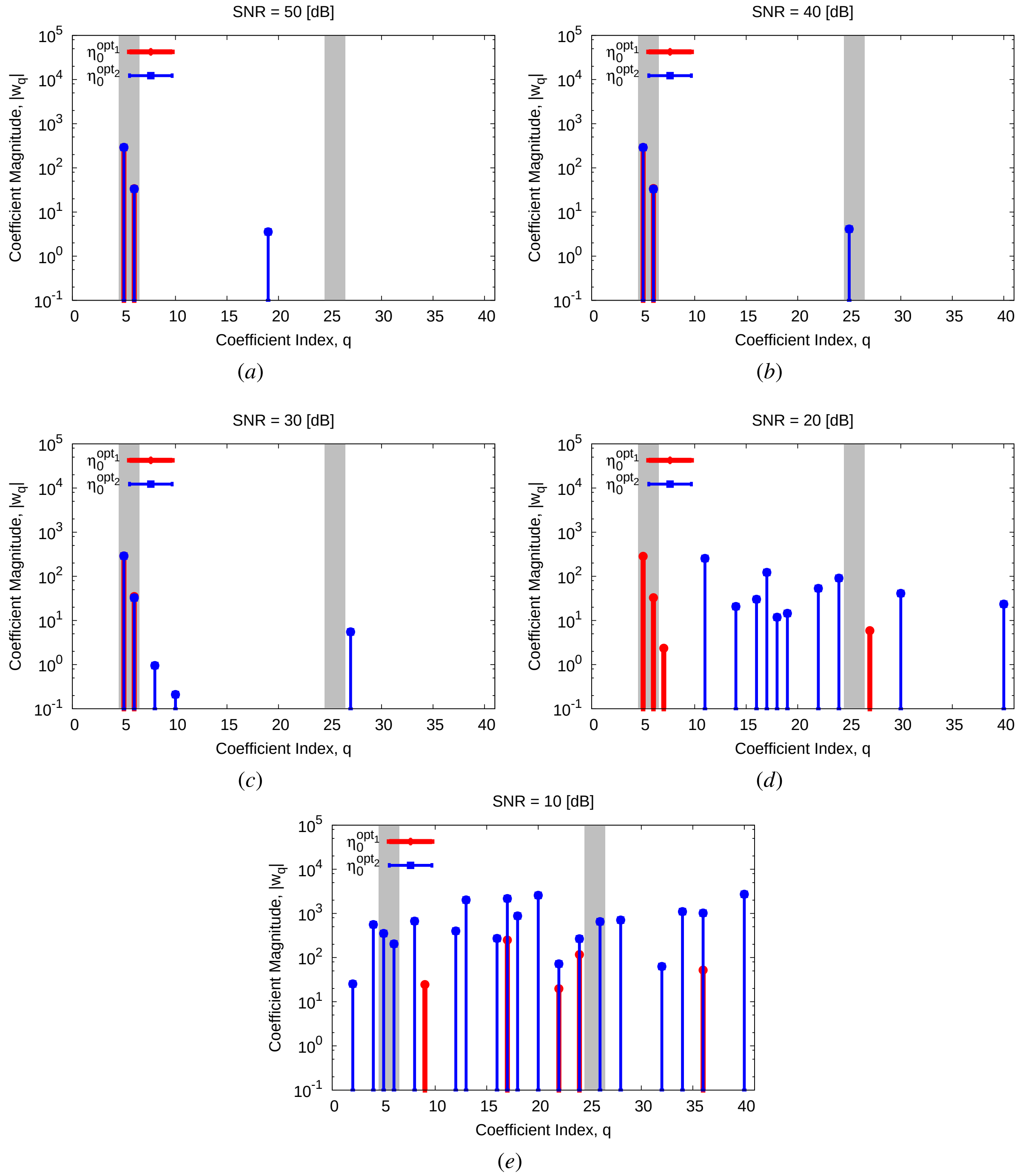

Figure 5: Vectors selected by the *BCS* solver

Observations

- The measured *AUT* has a failure of the excitation magnitude of the 3^{rd} row and for $SNR \geq 20\,[dB]$ the *BCS* solver is able to detect this failure. In particular, when $\eta_0^{opt_1}$ is used, the *BCS* is extremely precise in this failure detection for $SNR \geq 30\,[dB]$;
- on the other hand, the *BCS* solver is never able to find the phase failure affecting the *AUT*.

Estimated Near-Field $\eta_0^{\mathbf{opt_1}}$

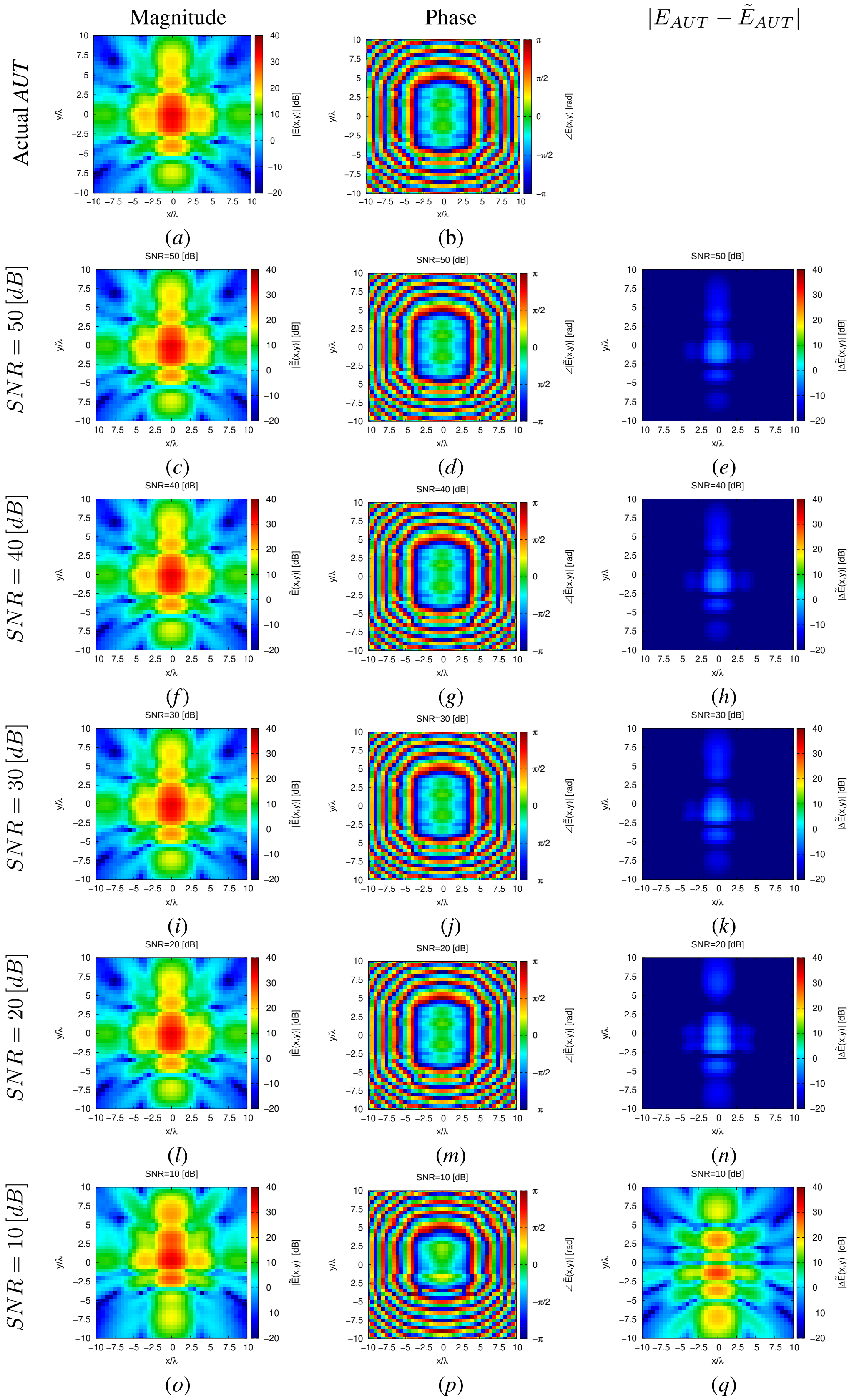

Figure 6: Magnitude and phase of the actual and estimated $2-D$ near-field pattern when processing noisy measurements at different SNRs.

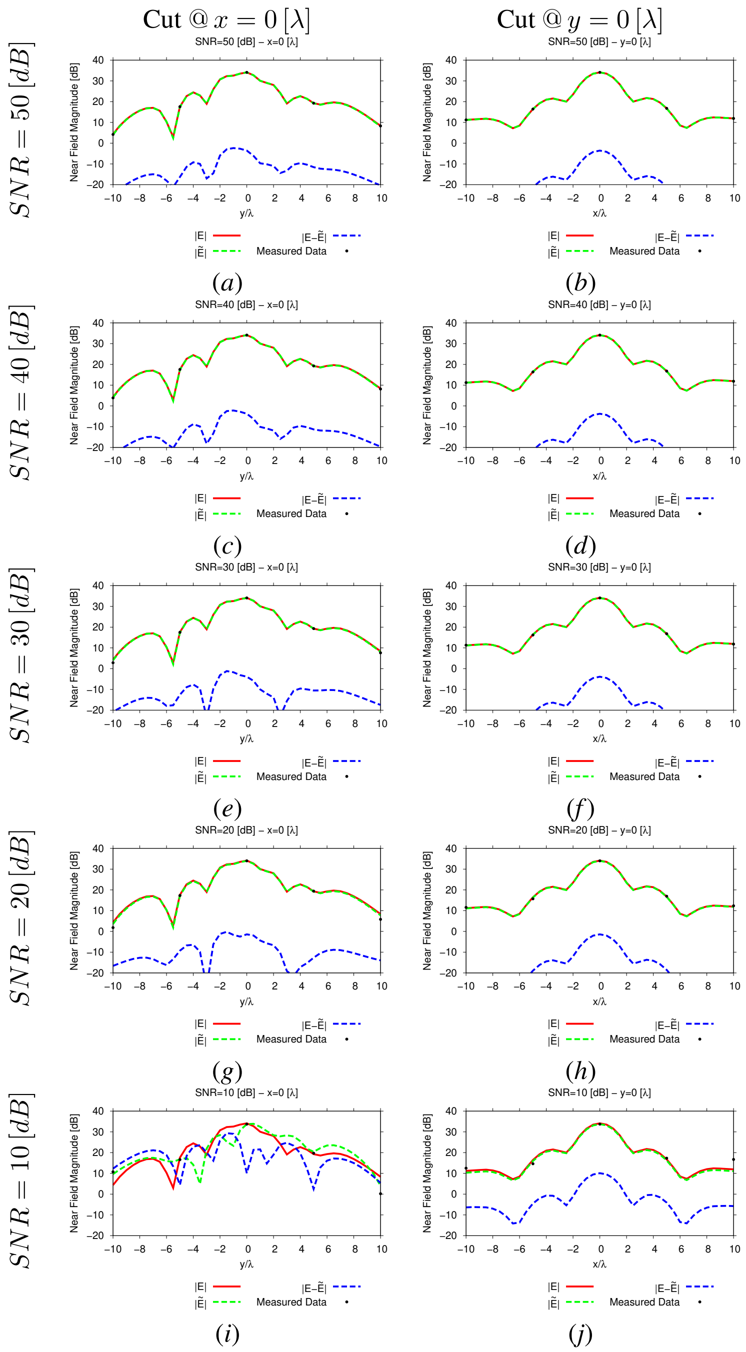

Figure 7: $1-D$ cuts of the estimated near-field pattern under several noisy conditions

Estimated Near-Field $\eta_0^{\mathbf{opt_2}}$

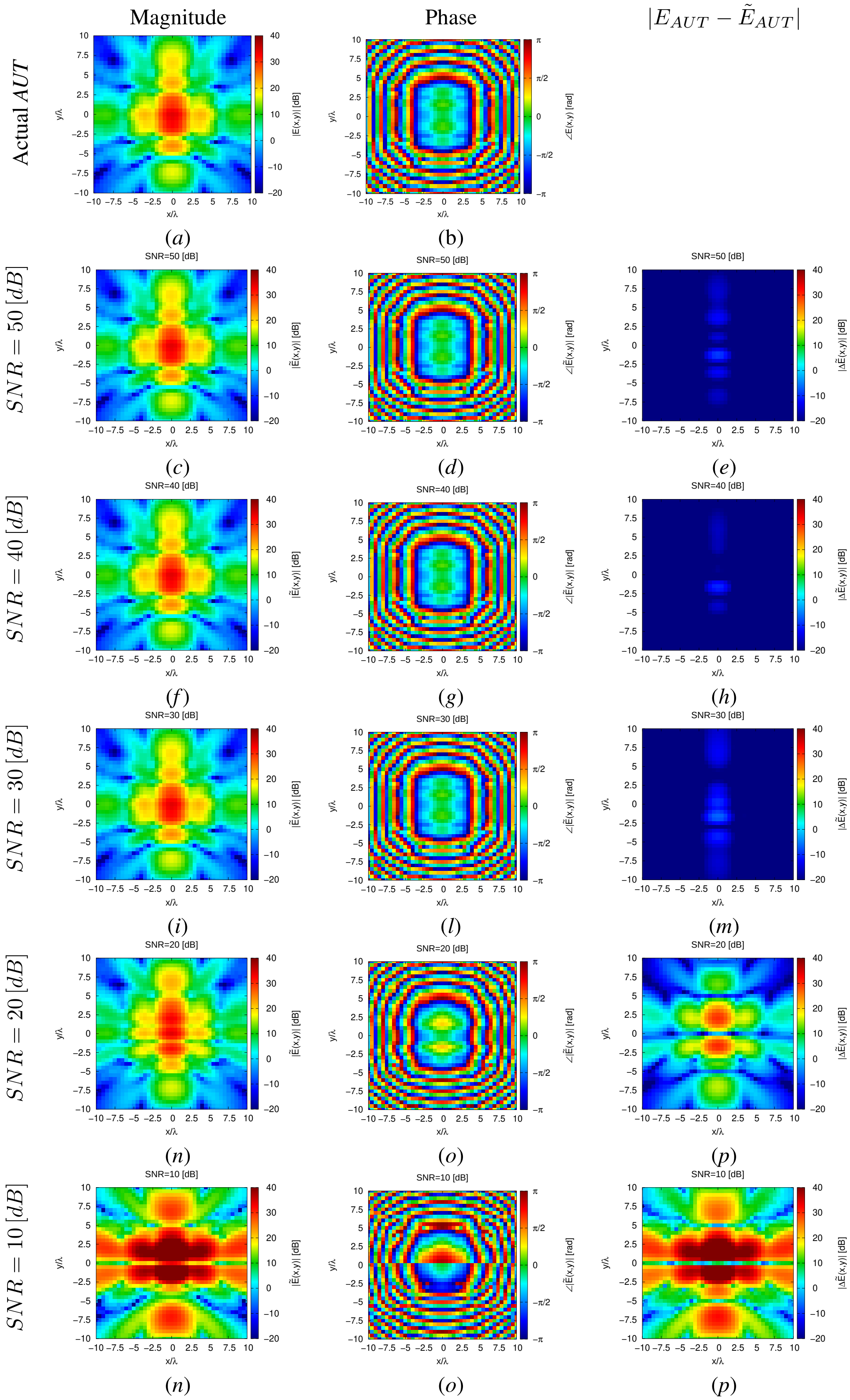

Figure 8: Magnitude and phase of the actual and estimated $2-D$ near-field pattern when processing noisy measurements at different SNRs.

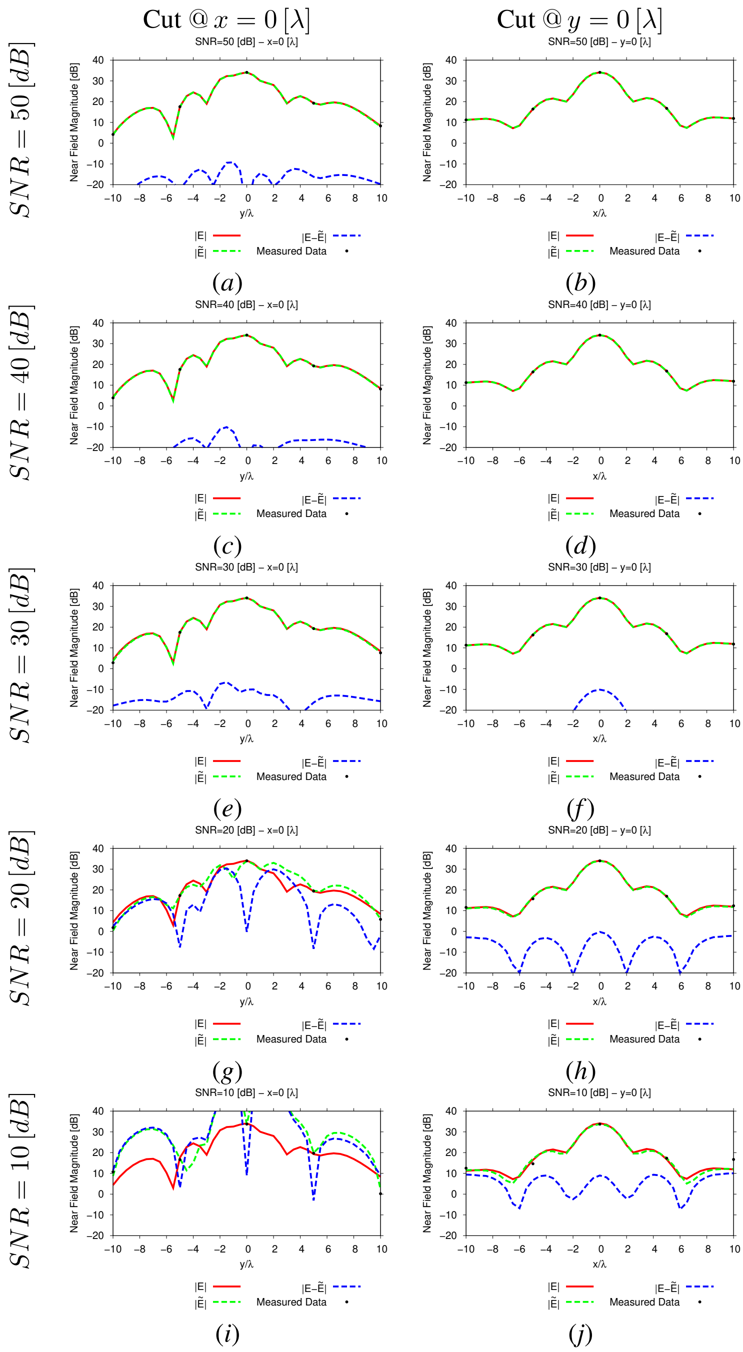

Figure 9: $1 - D$ cuts of the estimated near-field pattern under several noisy conditions

$SNR\,[dB]$	$Far-Field\,Error,\,\chi\ [dB]$	
	$\eta_0^{opt_1}$	$\eta_0^{opt_2}$
50	-36.25	-42.19
40	-36.24	-44.87
30	-36.04	-41.43
20	-39.29	-3.73
10	-4.90	3.81

Table II: Far-field matching error between the actual and estimated AUT patterns (both obtained through near-to-far-field transformation from the corresponding near-field patterns) under several noisy conditions.

Computational times

- Δt_{Sim}: Time required to simulate the K *AUT* configurations used to build the $(T \times K)$ "pattern matrix";
- Δt_{SVD}: Time required to perform the *SVD* of the $(T \times K)$ "pattern matrix";
- Δt_{MbE}^{BCS}: (Mean) Time required by the Measurement-by-Example tool to read the *SVD* output and perform the estimation of the *AUT* radiated field.

$\Delta t_{Sim}\ [sec]$	3.15×10^4
$\Delta t_{SVD}\ [sec]$	1.32×10^2
$\Delta t_{MbE}^{BCS}\ [sec]$	2.67×10^{-1}

Table III: Computational times

Remarks

- Given that the number of simulated *AUT*s is $K = S \times (F^{(3)} + P^{(3)}) = 120$, the average per-*AUT* simulation time is
$$\Delta t_{FEKO} \simeq \frac{\Delta t_{Sim}}{K} = \frac{3.15 \times 10^4}{120}\,[sec] = 2.62 \times 10^2\,[sec]$$

More information on the topics of this document can be found in the following list of references.

References

[1] M. Salucci, N. Anselmi, M. D. Migliore, and A. Massa, "A bayesian compressive sensing approach to robust near-field antenna characterization," *IEEE Trans. Antennas Propag.*, vol. 70, no. 9, pp. 8671-8676, Sep. 2022.

[2] B. Li, M. Salucci, W. Tang, and P. Rocca, "Reliable field strength prediction through an adaptive total-variation CS technique," *IEEE Antennas Wireless Propag. Lett.*, vol. 19, no. 9, pp. 1566-1570, Sep. 2020.

[3] M. Salucci, M. D. Migliore, P. Rocca, A. Polo, and A. Massa, "Reliable antenna measurements in a near-field cylindrical setup with a sparsity promoting approach," *IEEE Trans. Antennas Propag.*, vol. 68, no. 5, pp. 4143-4148, May 2020.

[4] G. Oliveri, M. Salucci, N. Anselmi, and A. Massa, "Compressive sensing as applied to inverse problems for imaging: theory, applications, current trends, and open challenges," *IEEE Antennas Propag. Mag.*, vol. 59, no. 5, pp. 34-46, Oct. 2017.

[5] A. Massa, P. Rocca, and G. Oliveri, "Compressive sensing in electromagnetics - A review," *IEEE Antennas Propag. Mag.*, vol. 57, no. 1, pp. 224-238, Feb. 2015.

[6] P. Rocca, N. Anselmi, M. A. Hannan, and A. Massa, "Conical frustum multi-beam phased arrays for air traffic control radars," *Sensors*, vol. 22, no. 19, 7309, pp. 1-18, 2022.

[7] F. Zardi, G. Oliveri, M. Salucci, and A. Massa, "Minimum-complexity failure correction in linear arrays via compressive processing," *IEEE Trans. Antennas Propag.*, vol. 69, no. 8, pp. 4504-4516, Aug. 2021.

[8] N. Anselmi, G. Gottardi, G. Oliveri, and A. Massa, "A total-variation sparseness-promoting method for the synthesis of contiguously clustered linear architectures," *IEEE Trans. Antennas Propag.*, vol. 67, no. 7, pp. 4589-4601, Jul. 2019.

[9] M. Salucci, A. Gelmini, G. Oliveri, and A. Massa, "Planar arrays diagnosis by means of an advanced bayesian compressive processing," *IEEE Tran. Antennas Propag.*, vol. 66, no. 11, pp. 5892-5906, Nov. 2018.

[10] L. Poli, G. Oliveri, P. Rocca, M. Salucci, and A. Massa, "Long-distance WPT unconventional arrays synthesis," *J. Electromagn. Waves Appl.*, vol. 31, no. 14, pp. 1399-1420, Jul. 2017.

[11] G. Oliveri, M. Salucci, and A. Massa, "Synthesis of modular contiguously clustered linear arrays through a sparseness-regularized solver," *IEEE Trans. Antennas Propag.*, vol. 64, no. 10, pp. 4277-4287, Oct. 2016.

[12] M. Carlin, G. Oliveri, and A. Massa, "Hybrid BCS-deterministic approach for sparse concentric ring isophoric arrays," *IEEE Trans. Antennas Propag.*, vol. 63, no. 1, pp. 378-383, Jan. 2015.

[13] G. Oliveri, E. T. Bekele, F. Robol, and A. Massa, "Sparsening conformal arrays through a versatile BCS-based method," *IEEE Trans. Antennas Propag.*, vol. 62, no. 4, pp. 1681-1689, Apr. 2014.

[14] F. Viani, G. Oliveri, and A. Massa, "Compressive sensing pattern matching techniques for synthesizing planar sparse arrays," *IEEE Trans. Antennas Propag*., vol. 61, no. 9, pp. 4577-4587, Sep. 2013.

[15] G. Oliveri, P. Rocca, and A. Massa, "Reliable diagnosis of large linear arrays - A bayesian compressive sensing approach," *IEEE Trans. Antennas Propag*., vol. 60, no. 10, pp. 4627-4636, Oct. 2012.

[16] G. Oliveri, M. Carlin, and A. Massa, "Complex-weight sparse linear array synthesis by bayesian compressive sampling," *IEEE Trans. Antennas Propag*., vol. 60, no. 5, pp. 2309-2326, May 2012.

[17] G. Oliveri and A. Massa, "Bayesian compressive sampling for pattern synthesis with maximally sparse non-uniform linear arrays," *IEEE Trans. Antennas Propag*., vol. 59, no. 2, pp. 467-481, Feb. 2011.

[18] P. Rocca, M. A. Hannan, M. Salucci, and A. Massa, "Single-snapshot DoA estimation in array antennas with mutual coupling through a multi-scaling BCS strategy," *IEEE Trans. on Antennas and Propag*., vol. 65, no. 6, pp. 3203-3213, Jun. 2017.

[19] M. Carlin, P. Rocca, G. Oliveri, F. Viani, and A. Massa, "Directions-of-arrival estimation through bayesian compressive sensing strategies," *IEEE Trans. Antennas Propag.*, vol. 61, no. 7, pp. 3828-3838, Jul. 2013.

[20] M. Carlin, P. Rocca, G. Oliveri, and A. Massa, "Bayesian compressive sensing as applied to directions-of-arrival estimation in planar arrays," *J. Electromagn. Waves Appl.*, vol. 2013, pp. 1-12, 2013.

[21] G. Oliveri, N. Anselmi, M. Salucci, L. Poli, and A. Massa, "Compressive sampling-based scattering data acquisition in microwave imaging," *J. Electromagn. Waves Appl.*, vol. 37, no. 5, 693-729, Mar. 2023.

[22] G. Oliveri, L. Poli, N. Anselmi, M. Salucci, and A. Massa, "Compressive sensing-based Born iterative method for tomographic imaging," *IEEE Tran. Microw. Theory Techn.*, vol. 67, no. 5, pp. 1753-1765, May 2019.

[23] M. Salucci, L. Poli, and G. Oliveri, "Full-vectorial 3D microwave imaging of sparse scatterers through a multi-task Bayesian compressive sensing approach," *J. Imag.*, vol. 5, no. 1, pp. 1-24, Jan. 2019.

[24] M. Salucci, A. Gelmini, L. Poli, G. Oliveri, and A. Massa, "Progressive compressive sensing for exploiting frequency-diversity in GPR imaging," *J. Electromagn. Waves Appl.*, vol. 32, no. 9, pp. 1164-1193, 2018.

[25] N. Anselmi, L. Poli, G. Oliveri, and A. Massa, "Iterative multi-resolution bayesian CS for microwave imaging," *IEEE Trans. Antennas Propag*., vol. 66, no. 7, pp. 3665-3677, Jul. 2018.

[26] N. Anselmi, G. Oliveri, M. A. Hannan, M. Salucci, and A. Massa, "Color compressive sensing imaging of arbitrary-shaped scatterers," *IEEE Trans. Microw. Theory Techn*., vol. 65, no. 6, pp. 1986-1999, Jun. 2017.

[27] N. Anselmi, G. Oliveri, M. Salucci, and A. Massa, "Wavelet-based compressive imaging of sparse targets," *IEEE Trans. Antennas Propag.*, vol. 63, no. 11, pp. 4889-4900, Nov. 2015.

[28] G. Oliveri, P.-P. Ding, and L. Poli "3D crack detection in anisotropic layered media through a sparseness-regularized solver," *IEEE Antennas Wireless Propag. Lett.*, vol. 14, pp. 1031-1034, 2015.

[29] L. Poli, G. Oliveri, P.-P. Ding, T. Moriyama, and A. Massa, "Multifrequency Bayesian compressive sensing methods for microwave imaging," *J. Opt. Soc. Am. A*, vol. 31, no. 11, pp. 2415-2428, 2014.

[30] G. Oliveri, N. Anselmi, and A. Massa, "Compressive sensing imaging of non-sparse 2D scatterers by a total-variation approach within the Born approximation," *IEEE Trans. Antennas Propag.*, vol. 62, no. 10, pp. 5157-5170, Oct. 2014.

[31] L. Poli, G. Oliveri, and A. Massa, "Imaging sparse metallic cylinders through a local shape function bayesian compressive sensing approach," *J. Opt. Soc. Am. A*, vol. 30, no. 6, pp. 1261-1272, 2013.

[32] L. Poli, G. Oliveri, F. Viani, and A. Massa, "MT-BCS-based microwave imaging approach through minimum-norm current expansion," *IEEE Trans. Antennas Propag.*, vol. 61, no. 9, pp. 4722-4732, Sep. 2013.

[33] F. Viani, L. Poli, G. Oliveri, F. Robol, and A. Massa, "Sparse scatterers imaging through approximated multitask compressive sensing strategies," *Microwave Opt. Technol. Lett.*, vol. 55, no. 7, pp. 1553-1558, Jul. 2013.

[34] L. Poli, G. Oliveri, P. Rocca, and A. Massa, "Bayesian compressive sensing approaches for the reconstruction of two-dimensional sparse scatterers under TE illumination," *IEEE Trans. Geosci. Remote Sensing*, vol. 51, no. 5, pp. 2920-2936, May 2013.

[35] L. Poli, G. Oliveri, and A. Massa, "Microwave imaging within the first-order Born approximation by means of the contrast-field Bayesian compressive sensing," *IEEE Trans. Antennas Propag.*, vol. 60, no. 6, pp. 2865-2879, Jun. 2012.

[36] G. Oliveri, L. Poli, P. Rocca, and A. Massa, "Bayesian compressive optical imaging within the Rytov approximation," *Optics Letters, vol.* 37, no. 10, pp. 1760-1762, 2012.

[37] G. Oliveri, P. Rocca, and A. Massa, "A Bayesian compressive sampling-based inversion for imaging sparse scatterers," *IEEE Trans. Geosci. Remote Sensing*, vol. 49, no. 10, pp. 3993-4006, Oct. 2011.